A pollen-climate calibration from western Patagonia for palaeoclimatic reconstructions

Vincent Montade, Odile Peyron, Charly Favier, Jean Pierre Francois, Simon Haberle

Article

A pollen-climate calibration from western Patagonia for palaeoclimatic reconstructions

J. Quaternary Sci., 2019, 34: 76-86. https://doi.org/10.1002/jqs.3082

Vincent Montade[1*], Odile Peyron[2], Charly Favier[2], Jean Pierre Francois[3], Simon G. Haberle[4,5]

[1]Department of Palynology and Climate Dynamics, Albrecht-von-Haller-Institute for Plant Sciences, Georg-August-University of Goettingen, Untere Karspüle 2, 37073 Goettingen, Germany

[2]ISEM, Univ. Montpellier, CNRS, EPHE, IRD, Montpellier, France

[3]Departamento de Ciencias Geográficas, Facultad de Ciencias Naturales y Exactas, Universidad de Playa Ancha, Leopoldo Carballo 270, Playa Ancha, Valparaíso, Chile.

[4]Department of Archaeology and Natural History, School of Culture, History and Language, College of Asia and the Pacific, Australian National University, Canberra, ACT 2601, Australia

[5]ARC Centre of Excellence for Australian Biodiversity and Heritage, Australian National University, Canberra, ACT 2601, Australia

*Corresponding author: Vincent Montade – vincent.montade@gmail.com

Abstract

Palaeoecological studies of sediment records in the western margins of southern South America have revealed the vegetation dynamic under the influence of major regional climate drivers such as the Southern Westerly Winds, Southern Annular Mode and the El Niño Southern Oscillation phenomenon. Despite the substantial number of palynological records that have been studied, very few quantitative pollen-based climate reconstructions using surface sample have been attempted. In this context, our objective is first to investigate the modern pollen-vegetation-climate relationships in the western Patagonian region. Results reveal that the modern pollen dataset reflects the main vegetation types and that summer precipitation and winter temperature represent the main climate parameters controlling vegetation distribution. Secondly using this pollen-climate dataset we evaluate and compare the performance of two models (Weighted Averaging Partial Least Squares and Modern Analog Technique). We applied these models to perform climate reconstructions from two oceanic pollen records from western Patagonia. Compared with independent climate indicators, our pollen pollen-inferred climate reconstructions reveal the same overall trends showing the potential of pollen–climate transfer functions applied to this region. This study provides much needed data for quantitative climate reconstructions in South America which still need to be improved by enlarging the modern pollen dataset.

Keywords

Palaeoclimate, Quantitative climate reconstruction, Pollen, western Patagonia, South America

1. Introduction

The latitudinal distribution of the main plant communities in western Patagonia closely follows the climate gradient across the region (Schmithüsen, 1956; Gajardo, 1994). In addition to temperatures decreasing southward, rainfall shows a strong increase southward directly related to the intensity of the Southern Westerly Wind (SWW) belt (Garreaud *et al.*, 2013). In particular, models and palaeoclimate archives reveal the importance of the SWW belt through their role in regional climate change, alongside the growing recognition of the role of the Southern Annular Mode and El Niño Southern Oscillation phenomenon in modulating regional climate through time (e.g. Toggweiler *et al.*, 2006; Anderson *et al.*, 2009; Moreno *et al.*, 2014). A substantial number of records based on palynological studies have thus been produced in this region with a focus on questions regarding the behaviour of the SWW belt at different timescales (see Flantua *et al.*, 2015 and literature therein). Western Patagonia is one of the regions from South America with the most pollen records and these studies have sometimes led to different conclusions regarding the long-term dynamics of the SWW belt (e.g. Kilian and Lamy, 2012). To explain those discrepancies new records are required in regions where the density of palaeoecological data is lower, such as in the Chilean channel region (47° to 53°S). On the other hand, to explain those discrepancies, it also requires improvement of the methods to reconstruct the climate. Indeed, most palaeodata from this region are based on qualitative climate reconstructions, which may limit the interpretation of multi-site comparisons for reconstructing climate variability at a regional scale. Quantitative climate approaches are thus needed to provide a better understanding of the regional pattern of climate changes. Such approaches are also essential to perform data-model comparisons improving our understanding of climate mechanisms and future climate changes (Harrison *et al.*, 2016). In Patagonia, local modern pollen datasets have been published during the last two decades to study relationships between pollen, vegetation and sometimes climate

(Haberle and Bennett, 2001; Paez *et al.*, 2001; Markgraf *et al.*, 2002; Tonello *et al.*, 2008, 2009; Mancini *et al.*, 2012; Schäbitz *et al.*, 2013). Only three local quantitative climate reconstructions inferred from fossil pollen records have been provided using some of these datasets (Markgraf *et al.*, 2002; Tonello *et al.*, 2009; Schäbitz *et al.*, 2013). Hence, further local studies calibrating the existing modern pollen data to perform quantitative reconstructions are necessary as a first step to large-scale regional climate reconstructions.

In this context our aim here is to compile modern pollen data from western Patagonia to investigate the modern pollen-vegetation-climate relationships and to develop climate transfer functions. We first assemble modern pollen samples to span the range of environmental values likely to be represented by the main different vegetation types from this region. Secondly, this paper aims to provide reliable quantitative estimates for seasonal climatic variables. Multiple methods for pollen-based climate reconstruction including most standard methods, the Weighted Averaging Partial Least Squares (WA-PLS) and the Modern Analog Technique (MAT) will be applied and compared. We finally use these models to perform quantitative climate reconstructions for the last deglaciation and the Holocene inferred from two pollen records: the core MD07-3104 in the Reloncaví Fjord at 41°S and the core MD07-3088 offshore Taitao Peninsula at 46°S (Montade *et al.*, 2012, 2013).

2. Environmental settings

Western Patagonia represents the southern part of South America in Southern Chile extending from 41° to 56°S (Fig. 1). The Andean Cordillera spreads from north to south with peaks rarely exceeding 3000 m asl. Along the coast, a secondary mountain range, the Coastal Range, is rapidly submerged south of 42°S which results in a complex system of fjords, channels and archipelagos. The combination of these mountain ranges with high-velocity SWW generates high orographic rainfall increasing southward with SWW intensity increase

(Garreaud *et al.*, 2013). During the austral winter the SWW belt spreads northward to 30°S but remains south of 46-47°S during the austral summer. In the northern part, precipitation primarily from winter rains, reaches around 2000 $mm.yr^{-1}$. Southwards, seasonality of precipitation decreases and disappears south of 46°S, where precipitation reaches values over 3000 $mm.yr^{-1}$. East of the Andes, the annual amount of precipitation decreases rapidly to below 1000 mm. The temperatures contrast with precipitation showing a weak annual seasonal variability with values remaining above freezing along the coast. However, with the altitude increase, temperature seasonality increases through the Andes. The climate is thus considered as temperate to cool-temperate and humid to hyper-humid from north to south at low elevation. East of the Andes, climate is generally dry and temperate to cool-temperate from north to south (Garreaud *et al.*, 2009).

Vegetation communities in western Patagonia are considered to be strongly influenced by the gradient of increasing annual precipitation and decreasing annual temperature southward (Schmithüsen, 1956; Gajardo, 1994; Markgraf *et al.*, 2002; Luebert and Pliscoff, 2004) (Fig. 1): (i) the Lowland Deciduous Forest, dominated by deciduous trees (i.e. *Nothofagus obliqua, N. alpina*), conifers (i.e. *Saxegothaea conspiscua, Podocarpus salignus*) and several broadleaf evergreen elements (i.e. *Aetoxicon punctatum, Persea lingue*); (ii) the Valdivian Rainforest, the most diversified Patagonian forest type, characterized by the codominance of evergreen trees (i.e. *Nothofagus dombeyi)* with a number of broadleaf evergreen elements (i.e. *Eucryphia cordifolia*, *Aetoxicon punctatum*, *Caldcluvia paniculata*, and several species of Myrtaceae); (iii) the North Patagonian Rainforest, dominated by several species of conifers (i.e. *Fitzroya cupressoides*, *Pilgerodendron uviferum*, *Podocarpus nubigenus*) with some *Nothofagus* and broadleaf species (i.e. *Nothofagus dombeyi, N. nitida, N. betuloides*, *Weinmannia trichosperma*); (iv) the Subantarctic Rainforest, characterized by the codominance of conifer and *Nothofagus* species (i.e. *Pilgerodendron uviferum*, *Nothofagus*

120 *nitida* and *N. betuloides*); (v) also frequently associated with the Subantarctic Rainforest, the
121 Magellanic Moorland represented by an open plant community occurring under high
122 precipitation is characterized by the predominance of peat-bog plants (i.e. *Sphagnum*
123 *magellanicum*), cushion-bog species (*Astelia pumila*, *Donatia fascicularis*) with graminoid
124 taxa mainly represented by Cyperaceae or Juncaceae and shrubs (Ericaceae); (vi) the
125 Subantarctic Deciduous Forest, mainly represented by deciduous trees (i.e. *Nothofagus*
126 *pumilio* and *N. antarctica*) adapted to cold conditions is also associated with an increase
127 proportion of graminoids (grasses or sedges) characteristic of to the Andean high elevation
128 grassland which dominates the landscape above the treeline.
129 Along the altitudinal gradient in northern Patagonia, with increasing orographic precipitation
130 and decreasing temperatures, a similar sequence of vegetation distribution is observed except
131 for the Magellanic Moorland which cannot develop under sub-zero temperature values.
132 Finally, east of the Andes under dry conditions the Patagonian Steppe develops in the
133 lowlands. The Patagonian Steppe is dominated by herbs and shrubs mainly characterized by
134 Poaceae, Asteraceae, Cyperaceae, Solanaceae, Apiaceae and Chenopodiaceae.
135

136 **3. Material and methods**

137 **3.1. Modern pollen and climate datasets**

138 The modern pollen dataset was compiled using 24 oceanic surface sediments (Montade *et al.*,
139 2011) and 186 terrestrial surface samples including 139 soils and 47 lakes (Haberle and
140 Bennett, 2001; Markgraf *et al.*, 2002; Francois, 2014). Much of these surface samples belong
141 to the northern half of Patagonia, distributed inland on both sides of the Andes (Fig. 1 and
142 Table S1). Only two samples are located between 47° and 52°S corresponding to oceanic
143 surface samples in the fjords. Further south, 19 samples are from islands within the fjords and
144 off-shore near Punta Arenas. After dataset compilation, a total of 78 pollen taxa was obtained

(Table S2) by updating the pollen taxa nomenclature followed the harmonization from Markgraf *et al.* (2002). To this initial harmonization, we added five pollen taxa related to samples located more southward (*Astelia*, *Caltha*, *Donatia*, *Lepidoceras*, *Luzuriaga*) and Asteraceae (except *Artemisia*) were merged in two groups: A. *Asteroideae* and A. *Cichorioideae*. For most of these samples, the pollen sums reach values above 200. Only 11 samples have a sum between 100 and 200; however as the number of surface samples is relatively limited, we decided to keep these samples in the dataset. Pollen percentages were calculated on the basis of their respective pollen sums excluding *Rumex* and Polygonaceae as these taxa are generally related to human impact (Heusser, 2003; Schäbitz *et al.*, 2013). Although characteristic of aquatic and wetland taxa some Cyperaceae species (sedges) are also naturally abundant in the Magellanic Moorland or in high elevation grasslands (Markgraf *et al.*, 2002; Villa-Martínez *et al.*, 2012). For that reason Cyperaceae was kept in the calculation of the pollen sums. To remove noise for statistical analyses, the data matrix was reduced to 38 taxa characterized by values above 2% in more than two samples. Furthermore, in order to provide a better understanding of the relationships between pollen assemblages, vegetation and climatic parameters from western Patagonia, statistical analyses were performed on a modern pollen dataset of 183 samples, excluding 27 samples from the initial dataset (Table S1). We first excluded samples dominated by herbs or shrubs pollen taxa located east of 71°W in northern half of Patagonia (north of 46°S) that mainly corresponds to Patagonian steppe controlled by the east-west climate Andean gradient. West of 71°W in northern half of Patagonia, we also excluded samples dominated by herbs or shrubs which correspond to samples influenced by human impact reflecting an open landscape vegetation at low elevation sites (< 500 m asl). We then excluded samples associated with pollen taxa of Magellanic Moorland from the same area, because their occurrences too far in the north reflect local edaphic conditions.

An unconstrained cluster analysis based on chord distance was performed on the 183 samples to reveal similarities among pollen assemblages and to provide the order of surface samples plotted in the pollen diagram (Fig. 2). The different pollen zones identified by the cluster dendrogram have been ascribed to groups according to pollen assemblages and vegetation types (Figs. 2 and 3). Climate data calculated at each surface sample location were extracted from the WorldClim database (Hijmans *et al.*, 2005). The present-day climate parameters correspond to the annual precipitation sum (P_{ANN}) and the precipitation sums during December-January-February (P_{SUM}) and June-July-August (P_{WIN}). Temperature values correspond to the mean values of the same months (T_{ANN}, T_{SUM} and T_{WIN}). For each oceanic sample, the closest on-shore climate values were calculated. In the Andes, because of the limited spatial resolution, elevational climate values based on WorldClim differ sometimes from the measured values by several hundred meters. As interpolated temperature values are very sensitive to the altitudinal gradient, we corrected temperature values using a lapse rate value of 0.6°C per 100 m. Altitude discrepancies were found to be too small to have a significant influence on precipitation estimates and no corrections have been done.

Based on the same modern pollen dataset, we carried out a Principal Component Analysis (PCA) on square-root transformed pollen relative frequencies and projected climate variables on it to determine if, and how, variation in pollen rain is related to climate patterns in western Patagonia. Square-root transformation of relative frequencies is commonly used as it allows variance stabilization and 'signal to noise' ratio maximization in the data (Prentice, 1980), which is equivalent to an ordination of pollen spectra using the square chord distance.

3.2. Quantitative climate reconstruction

The quantitative climate reconstruction is based on a multiple method approach to test the reliability of the methods for these complex environments and to provide an improved

assessment of the uncertainties involved in palaeoclimate reconstructions. Using the R package RIOJA (Juggins, 2015), we used the MAT based on a comparison of past assemblages to modern pollen assemblages, and the WA-PLS which requires statistical calibration. These methods are frequently used in climate reconstruction with their own set of advantages and limitations; they were successfully used for the Holocene climate reconstructions from terrestrial and marine records (e.g. Peyron *et al.*, 2011; Mauri *et al.*, 2015; Ortega-Rosas *et al.*, 2016). The MAT (Guiot, 1990) uses the squared-chord distance to determine the degree of similarity between samples with known climate parameters (modern pollen samples) to samples for which climate parameters are to be estimated (fossil pollen sample). The chord distance indicates the degree of dissimilarity between two pollen samples (small distance = close analogues selected for the climate reconstruction). A minimum distance corresponding to a minimum 'analogue' threshold is established. Subsequently, each climate parameter is calculated for each fossil pollen assemblage as the weighted mean of the climate of the closest modern analogues. The WA-PLS method (ter Braak and Juggins, 1993) is a transfer function which assumes that the relationship between pollen percentages and climate is unimodal. The modern pollen dataset used is considered a large matrix with n dimensions, corresponding to each of the pollen taxa within the dataset. WA-PLS operates by compressing the overall data structure into latent variables. Several taxa are directly related to climate parameters of interest. To avoid the co-linearity among the taxa, we can reduce the matrix into a smaller number of components based on both linear predictors of the parameter of interest and the residual structure of the data when those predictors are removed. The modification of PLS proposed by ter Braak and Juggins (1993) requires transformation of the initial dataset using weighted averaging along a gradient defined by the climate parameter of interest, such that the pollen taxa that best define the climate gradient are weighted more heavily than those that show little specificity to the gradient. Ter Braak and Juggins (1993)

detail the importance of using cross validation to assess and select WA-PLS models and show that statistics based on cross-validation provide more reliable measures of the true predictive ability of the transfer functions.

We then evaluate the performance of models using a leave-one-out cross-validation test performed with the training set of 183 modern pollen samples (38 pollen taxa). We also test the reliability of the transfer functions applied to oceanic pollen assemblages by reconstructing the climate conditions from 24 oceanic surface sediment samples (these oceanic samples were previously removed from the 183 modern pollen-climate training set before to do this test). We further check the extent to which calibration may be affected by spatial autocorrelation using the R package PALAEOSIG (Telford, 2015). Finally we apply the models to two oceanic pollen records: the core MD07-3104 located at 41°S in the Reloncaví Fjord and the core MD07-3088 located at 46°S offshore Taitao Peninsula (Montade *et al.*, 2012, 2013).

4. Results and discussion

4.1. Vegetation–pollen-climate relationships

The pollen spectra were divided into eleven zones according to the cluster analysis (Fig. 2). Because of limitations of morphological pollen identifications, most of the pollen taxa include several species, which explains the high proportion of some taxa in different pollen zones. In particular, the most abundant one, *Nothofagus dombeyi*-type includes five tree species (*N. dombeyi*, *N. pumilio*, *N. antarctica*, *N. betuloides*, *N. nitida*) growing in the different Patagonian environments. Based on the fluctuations of this pollen type associated and the dominant pollen taxa, we combined the pollen zones in six groups to reflect the main vegetation types and their ecological affinity (Figs. 2 and 3). In the grassland group which corresponds to three pollen zones, *Nothofagus dombeyi*-type remains below 20%. Samples are

245 generally dominated by at least one herbaceous taxon, reaching more than 25% (Poaceae,
246 Cyperaceae, Asteraceae *Asteroideae* or Apiaceae). Most of samples of this group occur in the
247 northern half of Patagonia in the Andes and correspond to an open landscape vegetation
248 characterized by high elevation grassland partly influenced by the Subantarctic Deciduous
249 Forest. Southward, samples that also corresponding to an open landscape vegetation are
250 associated with the Magellanic Moorland. Although characterized by different species, low
251 resolution pollen identification for non-arboreal taxa (mainly family) makes it difficult to
252 differentiate open vegetation between high elevation and lowland environments (Markgraf *et*
253 *al.*, 2002). Included in the same group, these samples from different environments reflect the
254 importance of precipitation variability (Fig. 3b) and winter temperatures, that are decreasing
255 with altitude or southward attaining low values in winter (~3°C). The Subantarctic Deciduous
256 Forest (SDF) group includes two pollen zones (Fig. 2), either dominated by *N. dombeyi*-type
257 (> 60%) or co-dominated by *N. dombeyi*-type (> 50%) and Cyperaceae (15-35%). These
258 assemblages are mainly distributed across the Andean relief in the northern half of Patagonia
259 with precipitation slightly higher and temperatures slightly lower than for the grassland group.
260 Samples co-dominated by Cyperaceae generally occurred above 900 m asl showing the
261 influence of high elevation grassland. Several samples are also located in the southern part
262 and five of them are from the islands within the fjords west of the Andes with high yearly
263 precipitation (Fig. 3). With two pollen zones, the Valdivian Rainforest (VR) group is
264 characterized by *N. dombeyi*-type remaining generally lower than 30%, accompanied by
265 significant amounts of arboreal taxa such as Myrtaceae, *Saxegothaea*, *Podocarpus*,
266 *Weinmannia* or *Gevuina/Lomatia*. Among herbaceous taxa only Poaceae reach values higher
267 than 10% in this group which could be partly induced by human impact in northwestern
268 Patagonia. Precipitation (2150 $mm.yr^{-1}$) and annual temperatures (10°C) in this region are
269 higher than in the two previous vegetation groups. The North Patagonian/Valdivian

Rainforest (NPR/VR) group (one pollen zone) shows again high amounts of *N. dombeyi*-type (> 50%), however the tree taxa *Podocarpus*, Cupressaceae, Myrtaceae and *Tepualia* replace herbaceous taxa in comparison with the SDF group. This group occurs in the northern half of Patagonia throughout the Andes and along the coast with generally high amounts of precipitation (2300 $mm.yr^{-1}$) and annual temperatures around 9°C. Only two samples from this group occur south of this domain probably related to their high frequencies of conifers. The North Patagonian/Subantarctic Rainforest (NPR/SR) group is represented by two pollen zones. It differs from NPR/VR group by lower values of *N. dombeyi*-type (< 40%) at the expense of Cupressaceae (max. up to 93%), *Podocarpus* and *Tepualia*. Samples are located in the same region than NPR/VR group with similar temperatures and slightly higher precipitation (2466 $mm.yr^{-1}$). Abundant in the NPR/VR and NPR/SR groups, the arboreal pollen taxon Cupressaceae includes three conifers, *Fitzroya cupressoides*, *Pilgerodendron uviferum* and *Austrocedrus chilensis*. The last one grows under colder and drier conditions than *F. cupressoides* and *P. uviferum* which are characteristic of very humid conditions mainly west of the Andes. Consequently, as discussed by Markgraf *et al.* (2002), the Cupressaceae pollen taxon may introduce some noise in climatic values of these two groups. In the Subantarctic Rainforest/Magellanic Moorland (SR/MM) group characterized by one pollen zone, pollen assemblages are mostly characterized by herbaceous or shrubby taxa with Ericales, *Myzodendron*, *Astelia*, Juncaceae and *Caltha* with *N. dombeyi*-type fluctuating between 30 and 50%. The pollen taxon *Astelia* characteristic of *A. pumila* only growing in the Magellanic Moorland is a very good indicator of this vegetation type. This group only occurs in southern Patagonia and the low seasonality of precipitation and temperature allows us to distinguish this vegetation group from the other ones (Fig. 3).

Distribution of samples in the PCA diagram (Fig. 4b) along the axis-1 reflects the variation from the vegetation in an open landscape (grassland and SR/MM groups) mixed with the SDF

group to the rainforest groups. Along axis-2, the distribution of samples mainly reflects the vegetation from the SR/MM, NPR/SR, NPR/VR groups to grassland and VR groups. Projection of climatic parameters in the PCA shows that the axis-1 is mainly correlated with temperatures while axis-2 is mainly correlated with precipitation (Fig. 4). In particular, the highest r^2 for axis-1 and -2 corresponding to T_{WIN} (0.55) and P_{SUM} (0.47), respectively, support the notion that parameters represent the main climatic limiting factors in western Patagonia determining vegetation distribution. This result is not surprising considering the vegetation distribution in western Patagonia which is characterized by a southward winter temperature decrease and a summer precipitation increase reducing rainfall seasonality (Fig. 1). A temperature decrease is also partly observed with altitude increase across the Andes in the northern half of western Patagonia where the rainforests is replaced by the SDF sometimes mixed with grasslands. Although we have a spatial gap in the sample distribution between 47° and 52°S, corresponding to the region where Magellanic Moorland mixed with the Subantarctic Rainforest is found, we partly capture the regional pattern of vegetation and climate conditions from this part of Patagonia with the samples located further south along the coast (52-53°S). In particular, under high annual rainfalls and a weak seasonality of precipitation and temperatures, these samples reflect similar climate and vegetation conditions with the region located from 47° to 48°S.

4.2. Model performance

4.2.1. Specificity of oceanic samples in western Patagonia

An important requirement in quantitative paleoenvironmental reconstruction is the need of a high-quality training set of modern samples. The training set should be (1) representative of the likely range of variables, (2) of highest possible taxonomy detail, (3) of comparable quality and (4) from the same sedimentary environment (Brewer *et al.*, 2013). The last point

can be particularly discussed because, due to our limited set of modern pollen samples, we decided to compile samples from different depositional environments (soil, lake and oceanic). Different depositional environment and taphonomic processes mainly between terrestrial and oceanic samples could affect significantly our pollen assemblages. Oceanic samples in particular should reflect a more regional signal than the terrestrial ones. However, it has been shown that the pollen signal from oceanic samples in this region remains relatively local to the vegetation from the nearby continental area (Montade *et al.*, 2011). This is mainly explained by the local transport conditions: under strong westerlies blowing throughout the year, the aeolian sediment input (including pollen) to the ocean is minimized and the pollen are mainly brought by strong fluvial discharges coming from short rivers restricting the sediment provenance. Probably partly related to these specific local conditions, it did not appear that these different depositional environments substantially affected pollen assemblages (Montade *et al.*, 2011).

To test the reliability of the transfer functions applied to oceanic pollen assemblages, we applied the WA-PLS and the MAT to the 24 oceanic surface sediment pollen samples, considered here as "fossil samples" (Fig. S1). The comparison between reconstructed and observed values for the main climatic limiting factor in western Patagonia, P_{SUM} and T_{WIN} shows a higher r^2 for the WA-PLS (0.56 and 0.67) than for the MAT (0.37 and 0.31). These correlations are explained by a general southward precipitation increase and temperature decrease, evidenced by both, reconstructed and observed values. However, some differences are observed. One of the most obvious concerns the reconstructed P_{SUM} values: while observed P_{SUM} reach maxima between 47° and 52°S, where the Subantarctic Rainforest mixed with the Magellanic Moorland occurs, the reconstructed values are much lower than observed. This may be explained by a lack of terrestrial samples between 47° and 52°S. In particular, the oceanic pollen samples at these latitudes are reconstructed with terrestrial samples from

Subantarctic Rainforest located to the north and not with the rainforest mixed with the Magellanic Moorland growing under very wet conditions. Concerning T_{WIN}, north of 47°S, reconstructed values are almost all underestimated. A large part of the terrestrial pollen dataset is located throughout the Andes, while the oceanic pollen dataset is located along the coast. Consequently temperature seasonality higher in the Andes induces lower reconstructed T_{WIN} than observed temperature along the coast. Despite these differences, explained by a lack of modern pollen samples, the MAT and the WA-PLS are able to reconstruct the general pattern of north-south climate gradient from oceanic pollen samples. Furthermore these results suggest that the WA-PLS seems more accurate than the MAT to reconstruct the overall latitudinal climate trends through western Patagonia.

4.2.2. Evaluation of the WA-PLS and the MAT models

After the first test on the oceanic pollen samples, we analysed the performance of the MAT and the WA-PLS transfer functions using the total 183-training set with a leave-one-out cross-validation. Prior to final model development, we checked for 'outliers', i.e. the modern pollen samples producing extreme values. Two outliers for P_{SUM} were identified in both, the MAT and the WA-PLS (Fig. S2). A third outlier was identified with P_{SUM} reconstructed by the WA-PLS showing a high negative value (ca. -500 mm). Such a value seems to be associated with a high percentage of *Araucaria* (>40%) reflecting a local signal from the vegetation. These three outliers were excluded from the training set. The final transfer functions was then performed on a 180-training set (Table 1 and Fig. 5). The optimal number of components to include in the WA-PLS model was assessed by a cross-validation following the procedure of ter Braak and Juggins (1993). A leave-one-out cross-validation has been selected here. A two component WA-PLS model was then selected on the basis of the low root mean square error of prediction (RMSEP), low maximum bias, and high r^2 between observed and predicted

values of P_{SUM} and T_{WIN} (Table 1). For the MAT, we retain the four nearest analogues for an optimal reconstruction.

The performance of our models is summarized in the Table 1. The RMSEP of the WA-PLS model is of ca. 164 mm for P_{SUM} and ca. 1.6°C for T_{WIN}. The r^2 between the observed climate values and those predicted by the WA-PLS (MAT) model is 0.53 (0.54) and 0.55 (0.77) for P_{SUM} and T_{WIN} respectively. Equivalent for P_{SUM}, the diagnostic statistics of MAT shows better scores for T_{WIN} mainly concerning the r^2. However, several studies suggest that MAT may produce over-optimistic diagnostics when cross-validation is limited to leave-one-out model (Telford and Birks, 2005). Low values of T_{WIN} are overestimated with both methods, particularly with the WA-PLS (Fig. 5). We also observed an underestimation of the high P_{SUM} values, particularly with the MAT.

The calibration seems robust and adequately model taxa and their environments with lowest possible error of prediction and the lowest bias values (Table 1). However, the good performance of the methods and the high correlations between climatic variables may also be discussed according to the potential problem of the spatial autocorrelation in transfer functions pointed out by Telford and Birks (2005). Spatial autocorrelation is the tendency of sites close to each other to resemble one another more than randomly selected sites. Telford and Birks (2005) argued that the estimation of the performance and the predictive power of a training set by cross-validation assume that the test set must be statistically independent of the training set and that a cross-validation in the presence of spatial-autocorrelation seriously violate this assumption as the samples are not always spatially and statistically independent. Therefore, in case of strong autocorrelation, the RMSEP on cross validation is overoptimistic. The importance of spatial autocorrelation in transfer functions evidenced by Telford and Birks (2005) has been discussed by several authors (Telford and Birks, 2005; Guiot and de Vernal, 2007; Fréchette *et al.*, 2008; Thompson *et al.*, 2008). However, the problems of

autocorrelation in evaluation models are rarely tested in transfer functions inferred from pollen data (Fréchette *et al.*, 2008; Cao *et al.*, 2014; Tian Fang *et al.*, 2014), although these analyses are essential to obtain a robust transfer function.

Therefore to check if spatial autocorrelation affects the western Patagonia training set we have used the graphical method developed by Telford and Birks (2009). We compare the performance of the WA-PLS and MAT as the training set size is reduced by deleting sites at random, and by deleting sites geographically and environmentally close to the test site in cross-validation (Fig. S3). In the case of autocorrelation, deleting geographically close sites will preferentially delete the best analogues, and worsen the performance statistics more than random deletion. If the observations are independent, deleting a given proportion of them should have the same effect regardless of how they are selected (Telford and Birks, 2009). Our results suggest that the r^2 from deleting of geographical neighbourhood sites closely follow the r^2 from deleting the environmental neighbourhood sites indicating that P_{SUM} and T_{WIN} are influenced by autocorrelation. The r^2 scores strongly decrease after 40 km for P_{SUM} and after 80 km for T_{WIN} and suggest that T_{WIN} seems to be less affected by autocorrelation than P_{SUM}. This strong r^2 decrease shows that if a large amount of sites are deleted from the training set, the transfer functions are strongly affected by a lack of sample. This highlight the limited size of our training set from a region characterized by a complex environmental and vegetation gradient. In that case an enlarged dataset would be necessary to more rigorously perform model cross-validation and to address more fully these problems of spatial autocorrelation. However, another way to check the reliability of our models is to apply it to fossil pollen data and to compare the signal with independent proxies.

4.3. Application of WA-PLS and the MAT to fossil pollen records

Here we applied the WA-PLS and the MAT to two oceanic pollen records, core MD07-3088 located at 46°S off Taitao Peninsula and core MD07-3104 located at 41°S in Reloncaví Fjord (Figs. 1 and 6). Spanning the last deglaciation and the Holocene, pollen data from core MD07-3088 illustrate the development of the North Patagonian Rainforest, which is interrupted by an expansion of Magellanic Moorland during the Antarctic Cold Reversal (ACR) (Montade *et al.*, 2013). Located further north, the core MD07-3104 shows compositional changes of temperate rainforest indicating warm and dry conditions during the beginning of the Holocene and more climate variability from the mid-Holocene associated with a cooling trend and with an increase of precipitation (Montade *et al.*, 2012). Although the climate reconstructions based on both models are consistent, the minor fluctuations indicated by the MAT do not evidence significant climate changes. As previously mentioned, this confirms that the MAT seems less appropriate than the WA-PLS to provide reliable climate reconstructions according to our modern pollen-climate dataset. For that reason, the climate reconstructions discussed below are based on the WA-PLS results.

Before 18 kyr, results obtained from core MD07-3088 at 46°S indicate lower values than modern ones for P_{SUM} (400-300 mm) and T_{WIN} (ca. 3°C). However, before 18 kyr, these results must be taken with caution given that during the late glacial, the pollen signal is characterized by low pollen concentrations reflecting reduced or absent vegetation on the adjacent land areas at a time, and the potential for non-analogue vegetation communities to be present during the glacial and post-glacial transition, when glaciers were greatly expanded compared to the present (Montade *et al.*, 2013). Under these conditions an overrepresentation of high producers of pollen such as *Nothofagus* trees was observed, which prevents local vegetation reconstructions and which is likely to bias our climate reconstructions at that time. From 18-17.5 kyr, a slight warming trend of 0.5°C is recorded, contemporaneous of the beginning of the deglaciation evidenced by the δD variations of EPICA Dome C ice core (Fig.

6d). Such a trend occurs simultaneously with the development of vegetation following the retreat of glaciers recorded in the region (Bennett *et al.*, 2000; Haberle and Bennett, 2004). Recorded from the same core, the beginning of the last deglaciation is also well evidenced by the increase of summer sea surface temperature (SSTs, Fig. 6c) reconstructed from planktonic foraminifera assemblages (Siani *et al.*, 2013). The strongest change evidenced by our climate reconstruction correspond to a rapid P_{SUM} increase starting at 14.5 kyr (ACR) with maximum values between 800 and 1000 mm. High P_{SUM} values persist up to the end of the Younger Dryas (YD) period (Fig. 6c). Simultaneously, we observe a progressive T_{WIN} increase of ca. 2°C while for the SSTs, values stop to increase during the ACR then decrease of 1°C at 13 kyr before to reach maxima after the YD. This strong precipitation increase characterised by very high values suggests an intensification of the SWW during the ACR and the YD. Already recorded by previous studies from western Patagonia, this abrupt change was interpreted as a northward shift of the SWW belt (García *et al.*, 2012; Moreno *et al.*, 2012; Montade *et al.*, 2015). Today, latitudes under the core of the SWW belt where rainfalls are very high, the temperature seasonality is the lowest of western Patagonia and, because of strong ocean influence, temperature values remain always positive at low elevation. Consequently, after the last glacial conditions, such an intensification of SWW and precipitation would have reduced the temperature seasonality inducing a milder summer and winter temperature. This scenario might explain the observed T_{WIN} increase by our reconstruction. Based on this result, glacier advances evidenced in western Patagonia during the ACR and the YD might be more related to hydrological changes than to a strong cooling (Moreno *et al.*, 2009; García *et al.*, 2012; Glasser *et al.*, 2012). However, additional quantitative climate reconstructions are necessary to test this hypothesis.

After the YD, P_{SUM} reconstructed from core MD07-3088 decrease progressively to reach present-day values between 400 and 500 mm (Fig. 6a). T_{WIN} values (ca. 6°C) are maxima

during the early Holocene, before they slightly decrease and fluctuate between 5 and 6°C, close to modern values (Fig. 6c). This moderate change in comparison with the last deglaciation are consistent with past vegetation dynamics recorded from the same latitude showing that the North Patagonian Rainforest rapidly reaches its modern composition during the early Holocene (Bennett *et al.*, 2000). On the other hand, the core MD07-3104 indicates a stronger climate variability during the Holocene. After reaching their maxima after the YD, P_{SUM} and T_{WIN} decrease from 500 to 350 mm and from 11 to 8.5°C from the early to the mid-Holocene (Figs. 6a and c). Then from 6 kyr, P_{SUM} and T_{WIN} fluctuate around 400 mm and 9°C before a slight decrease during the late Holocene to reach values close to the modern conditions. The climate variability reconstructed from core MD07-3104 is compared with a pollen index calculated from Lago Condorito located at ca. 30 km from the oceanic core (Moreno, 2004; Moreno *et al.*, 2010). Based on the normalized ratio between *Eucryphia-Caldcluvia* and *Podocarpus*, positive values of this index reflect a warm-temperate, seasonally dry climate with reduced SWW and negative values indicate cool-temperate and/or wet conditions with enhanced SWW. While our reconstruction indicates that T_{WIN} increase is associated with P_{SUM} increase, the pollen index indicates warm-temperate conditions under low precipitation (Fig. 6). This difference might be related to a different sensitivity of seasonality between the pollen index and our reconstructed T_{WIN}. On the other hand, comparison of P_{SUM} curve and the index reveals the same trend. Although a short time lag is observed, which is certainly related to a problem of marine age reservoir from the oceanic core (Montade *et al.*, 2012), our P_{SUM} reconstruction supports the known dynamic of precipitation and SWW changes in the region. Southward at 46°S, such changes are not recorded by our climate reconstruction and by vegetation changes (Montade *et al.*, 2013). Today the northern Patagonia at 41°S is characterized by a seasonally dry climate directly connected with a strong seasonality of SWW intensity. In comparison, the location of core

MD07-3088 closer to the position of the core of SWW already since the early Holocene, under the persistent influence of the SWW, rainfalls are strong all over the year. Consequently, this might explain why hydrological changes related to SWW changes would have more impacted the northern Patagonia during the Holocene.

Conclusions

To conclude, although based on different depositional environments (soil, lake and ocean), our modern pollen dataset (183 samples) from western Patagonia reflects the main vegetation types distributed along the latitudinal and the altitudinal gradient. Investigating the modern pollen-vegetation-climate relationships, we further demonstrate that the major vegetation distribution reflected by pollen assemblages is mainly controlled by two parameters: P_{SUM} and T_{WIN}. Characterized by a southward T_{WIN} decrease and a southward P_{SUM} increase, these two parameters represent the main climatic limiting factor in western Patagonia controlling the latitudinal distribution of the vegetation. Based on the modern pollen dataset, we then analysed and compared the performance of two standard methods: the MAT and the WA-PLS. They adequately model taxa and their environments; however our results also reveal that the WA-PLS is more suitable than the MAT which suffers of a lack of modern pollen samples to perform reliable climate reconstructions. Using two oceanic cores from northern Patagonia at 41°S and 46°S we finally proceeded to reconstructions of P_{SUM} and T_{WIN} values during the late Glacial and the Holocene. The most important climate change occurred during ACR and YD where P_{SUM} reach the double amount of modern values related to an enhanced SWW. Although our results show several methodological limitations (mainly by using oceanic and terrestrial samples together), our climate reconstructions, consistent with the regional climate changes, illustrate the potential to develop quantitative methods in western Patagonia. Representing one of the parts of South America with the most pollen records, additional

519 quantitative climate reconstructions have to be performed to improve our understanding of
520 climate dynamic at a regional scale. Furthermore, the modern pollen dataset still needs to be
521 enlarged, to reduce uncertainties of climate reconstructions.
522
523 **Acknowledgements**
524 V.M. benefited from a postdoctoral position funded by Ecole Pratique des Hautes Etudes at
525 Institut des Sciences de l'Evolution de Montpellier (ISEM) and Deutsche
526 Forschungsgemeinschaft at Department of Palynology and Climate Dynamics from the
527 University of Goettingen. We thank Vera Markgraf for sharing pollen data and for helpful
528 comments on the first version of the manuscript. We also thank Elisabeth Michel and
529 Giuseppe Siani for sharing data concerning the oceanic core MD07-3088. Finally we are
530 particularly grateful from the very constructive comments from two anonymous referees
531 greatly improving this manuscript. This is an ISEM contribution n°XX.
532
533 **References**
534 Anderson RF, Ali S, Bradtmiller LI, Nielsen SHH, Fleisher MQ, Anderson BE, Burckle LH.
535 2009. Wind-Driven Upwelling in the Southern Ocean and the Deglacial Rise in
536 Atmospheric CO_2. *Science* **323**: 1443–1448.
537 Bennett KD, Haberle SG, Lumley SH. 2000. The Last Glacial-Holocene Transition in
538 Southern Chile. *Science* **290**: 325–328.
539 ter Braak CJF, Juggins S. 1993. Weighted averaging partial least squares regression (WA-
540 PLS): an improved method for reconstructing environmental variables from species
541 assemblages. *Hydrobiologia* **269**–**270**: 485–502.

Brewer S, Guiot J, Barboni D. 2013. POLLEN METHODS AND STUDIES | Use of Pollen as Climate Proxies. In *Encyclopedia of Quaternary Science (Second Edition)*, Elias SA, Mock CJ (eds). Elsevier: Amsterdam; 805–815.

Cao X, Herzschuh U, Telford RJ, Ni J. 2014. A modern pollen–climate dataset from China and Mongolia: Assessing its potential for climate reconstruction. *Review of Palaeobotany and Palynology* **211**: 87–96.

Flantua SGA, Hooghiemstra H, Grimm EC, Behling H, Bush MB, González-Arango C, Gosling WD, Ledru M-P, Lozano-García S, Maldonado A, Prieto AR, Rull V, Van Boxel JH. 2015. Updated site compilation of the Latin American Pollen Database. *Review of Palaeobotany and Palynology* **223**: 104–115.

Francois J-P. 2014. *Postglacial paleoenvironmental history of the Southern Patagonian Fjords at 53°S.* PhD thesis. Universität zu Köln.

Fréchette B, de Vernal A, Guiot J, Wolfe AP, Miller GH, Fredskild B, Kerwin MW, Richard PJH. 2008. Methodological basis for quantitative reconstruction of air temperature and sunshine from pollen assemblages in Arctic Canada and Greenland. *Quaternary Science Reviews* **27**: 1197–1216.

Gajardo R. 1994. *La vegetación natural de Chile : clasificación y distribución geográfica.* Santiago.

García JL, Kaplan MR, Hall BL, Schaefer JM, Vega RM, Schwartz R, Finkel R. 2012. Glacier expansion in southern Patagonia throughout the Antarctic cold reversal. *Geology* **40**: 859–862.

Garreaud R, Lopez P, Minvielle M, Rojas M. 2013. Large-Scale Control on the Patagonian Climate. *Journal of Climate* **26**: 215–230.

Garreaud RD, Vuille M, Compagnucci R, Marengo J. 2009. Present-day South American climate. *Palaeogeography, Palaeoclimatology, Palaeoecology* **281**: 180–195.

Glasser NF, Harrison S, Schnabel C, Fabel D, Jansson KN. 2012. Younger Dryas and early Holocene age glacier advances in Patagonia. *Quaternary Science Reviews* **58**: 7–17.

Grieser J, Giommes R, Bernardi M. 2006. New_LocClim - the Local Climate Estimator of FAO. *Geophysical Research Abstracts* **8**: 08305.

Guiot J. 1990. Methodology of the last climatic cycle reconstruction in France from pollen data. *Palaeogeography, Palaeoclimatology, Palaeoecology* **80**: 49–69.

Guiot J, de Vernal A. 2007. Chapter Thirteen Transfer Functions: Methods for Quantitative Paleoceanography Based on Microfossils. In *Developments in Marine Geology*, Hillaire–Marcel C, de Vernal A. (eds). Elsevier: Amsterdam; 523–563.

Haberle SG, Bennett KD. 2001. Modern pollen rain and lake mud-water interface geochemistry along environmental gradients in southern Chile. *Review of Palaeobotany and Palynology* **117**: 93–107.

Haberle SG, Bennett KD. 2004. Postglacial formation and dynamics of North Patagonian Rainforest in the Chonos Archipelago, Southern Chile. *Quaternary Science Reviews* **23**: 2433–2452.

Harrison SP, Bartlein PJ, Prentice IC. 2016. What have we learnt from palaeoclimate simulations? *Journal of Quaternary Science* **31**: 363–385.

Heusser CJ. 2003. *Ice age Southern Andes - A chronicle of paleoecological events*. Elsevier: Amsterdam.

Hijmans RJ, Cameron SE, Parra JL, Jones PG, Jarvis A. 2005. Very high resolution interpolated climate surfaces for global land areas. *International Journal of Climatology* **25**: 1965–1978.

Juggins PS. 2015. rioja: Analysis of Quaternary Science Data. *http://eprints.ncl.ac.uk*.

Kilian R, Lamy F. 2012. A review of Glacial and Holocene paleoclimate records from southernmost Patagonia (49–55°S). *Quaternary Science Reviews* **53**: 1–23.

592 Lemieux-Dudon B, Blayo E, Petit J-R, Waelbroeck C, Svensson A, Ritz C, Barnola J-M,
593 Narcisi BM, Parrenin F. 2010. Consistent dating for Antarctic and Greenland ice
594 cores. *Quaternary Science Reviews* **29**: 8–20.
595 Luebert F, Pliscoff P. 2004. *Classification de pisios de vegetatacion y anlysis de*
596 *representatividad ecologica de areas propuesta para la proteccion en la ecoregion*
597 *valdivia.* Santiago.
598 Mancini MV, de Porras ME, Bamonte FP. 2012. Southernmost South America Steppes:
599 vegetation and its modern pollen-assemblages representation. In *Steppe Ecosystem*
600 *Dynamics, Land Use and Conservation*, Germano D (ed). Nova Science Publishers:
601 New York; 141–156.
602 Markgraf V, Webb RS, Anderson KH, Anderson L. 2002. Modern pollen/climate calibration
603 for southern South America. *Palaeogeography, Palaeoclimatology, Palaeoecology*
604 **181**: 375–397.
605 Mauri A, Davis BAS, Collins PM, Kaplan JO. 2015. The climate of Europe during the
606 Holocene: a gridded pollen-based reconstruction and its multi-proxy evaluation.
607 *Quaternary Science Reviews* **112**: 109–127.
608 Montade V, Combourieu-Nebout N, Chapron E, Mulsow S, Abarzúa AM, Debret M, Foucher
609 A, Desmet M, Winiarski T, Kissel C. 2012. Regional vegetation and climate changes
610 during the last 13 kyr from a marine pollen record in Seno Reloncaví, southern Chile.
611 *Review of Palaeobotany and Palynology* **181**: 11–21.
612 Montade V, Combourieu-Nebout N, Kissel C, Haberle SG, Siani G, Michel E. 2013.
613 Vegetation and climate changes during the last 22,000 yr from a marine core near
614 Taitao Peninsula, southern Chile. *Palaeogeography, Palaeoclimatology,*
615 *Palaeoecology* **369**: 335–348.

Montade V, Combourieu-Nebout N, Kissel C, Mulsow S. 2011. Pollen distribution in marine surface sediments from Chilean Patagonia. *Marine Geology* **282**: 161–168.

Montade V, Kageyama M, Combourieu-Nebout N, Ledru M-P, Michel E, Siani G, Kissel C. 2015. Teleconnection between the Intertropical Convergence Zone and southern westerly winds throughout the last deglaciation. *Geology* **43**: 735–738.

Moreno PI. 2004. Millennial-scale climate variability in northwest Patagonia over the last 15 000 yr. *Journal of Quaternary Science* **19**: 35–47.

Moreno PI, Francois JP, Moy CM, Villa-Martínez R. 2010. Covariability of the Southern Westerlies and atmospheric CO_2 during the Holocene. *Geology* **38**: 727–730.

Moreno PI, Kaplan MR, Francois JP, Villa-Martinez R, Moy CM, Stern CR, Kubik PW. 2009. Renewed glacial activity during the Antarctic cold reversal and persistence of cold conditions until 11.5 ka in southwestern Patagonia. *Geology* **37**: 375–378.

Moreno PI, Vilanova I, Villa-Martínez R, Garreaud RD, Rojas M, De Pol-Holz R. 2014. Southern Annular Mode-like changes in southwestern Patagonia at centennial timescales over the last three millennia. *Nature Communications* **5**: 4375.

Moreno PI, Villa-Martínez R, Cárdenas ML, Sagredo EA. 2012. Deglacial changes of the southern margin of the southern westerly winds revealed by terrestrial records from SW Patagonia (52°S). *Quaternary Science Reviews* **41**: 1–21.

Ortega-Rosas CI, Peñalba MC, Guiot J. 2016. The Lateglacial interstadial at the southeastern limit of the Sonoran Desert, Mexico: vegetation and climate reconstruction based on pollen sequences from Ciénega San Marcial and comparison with the subrecent record. *Boreas* **45**: 773–789.

Paez MM, Schäbitz F, Stutz S. 2001. Modern pollen–vegetation and isopoll maps in southern Argentina. *Journal of Biogeography* **28**: 997–1021.

640 Peyron O, Goring S, Dormoy I, Kotthoff U, Pross J, de Beaulieu J-L, Drescher-Schneider R,
641 Vannière B, Magny M. 2011. Holocene seasonality changes in the central
642 Mediterranean region reconstructed from the pollen sequences of Lake Accesa (Italy)
643 and Tenaghi Philippon (Greece). *The Holocene* **21**: 131–146.
644 Prentice IC. 1980. Multidimensional scaling as a research tool in quaternary palynology: A
645 review of theory and methods. *Review of Palaeobotany and Palynology* **31**: 71–104.
646 Schäbitz F, Wille M, Francois J-P, Haberzettl T, Quintana F, Mayr C, Lücke A, Ohlendorf C,
647 Mancini V, Paez MM, Prieto AR, Zolitschka B. 2013. Reconstruction of
648 palaeoprecipitation based on pollen transfer functions – the record of the last 16 ka
649 from Laguna Potrok Aike, southern Patagonia. *Quaternary Science Reviews* **71**: 175–
650 190.
651 Schmithüsen J. 1956. Die räumliche Ordnung der chilenischen Vegetation. *Bonner*
652 *Geographische Abhandlungen* **17**: 1–86.
653 Siani G, Michel E, De Pol-Holz R, DeVries T, Lamy F, Carel M, Isguder G, Dewilde F,
654 Lourantou A. 2013. Carbon isotope records reveal precise timing of enhanced
655 Southern Ocean upwelling during the last deglaciation. *Nature Communications* **4**.
656 Telford RJ. 2015. *palaeoSig: Significance Tests for Palaeoenvironmental Reconstructions.*
657 Telford RJ, Birks HJB. 2005. The secret assumption of transfer functions: problems with
658 spatial autocorrelation in evaluating model performance. *Quaternary Science Reviews*
659 **24**: 2173–2179.
660 Telford RJ, Birks HJB. 2009. Evaluation of transfer functions in spatially structured
661 environments. *Quaternary Science Reviews* **28**: 1309–1316.
662 Thompson RS, Anderson KH, Bartlein PJ. 2008. Quantitative estimation of bioclimatic
663 parameters from presence/absence vegetation data in North America by the modern
664 analog technique. *Quaternary Science Reviews* **27**: 1234–1254.

Tian F, Herzschuh U, Telford RJ, Mischke S, Van der Meeren T, Krengel M, Richardson J. 2014. A modern pollen–climate calibration set from central-western Mongolia and its application to a late glacial–Holocene record. *Journal of Biogeography* **41**: 1909–1922.

Toggweiler JR, Russell JL, Carson SR. 2006. Midlatitude westerlies, atmospheric CO_2, and climate change during the ice ages. *Paleoceanography* **21**: 1–15.

Tonello MS, Mancini MV, Seppä H. 2009. Quantitative reconstruction of Holocene precipitation changes in southern Patagonia. *Quaternary Research* **72**: 410–420.

Tonello MS, Prieto AR. 2008. Modern vegetation-pollen-climate relationships for the Pampa grasslands of Argentina. *Journal of Biogeography* **35**: 926–938.

Villa-Martínez R, Moreno PI, Valenzuela MA. 2012. Deglacial and postglacial vegetation changes on the eastern slopes of the central Patagonian Andes (47°S). *Quaternary Science Reviews* **32**: 86–99.

Figure caption

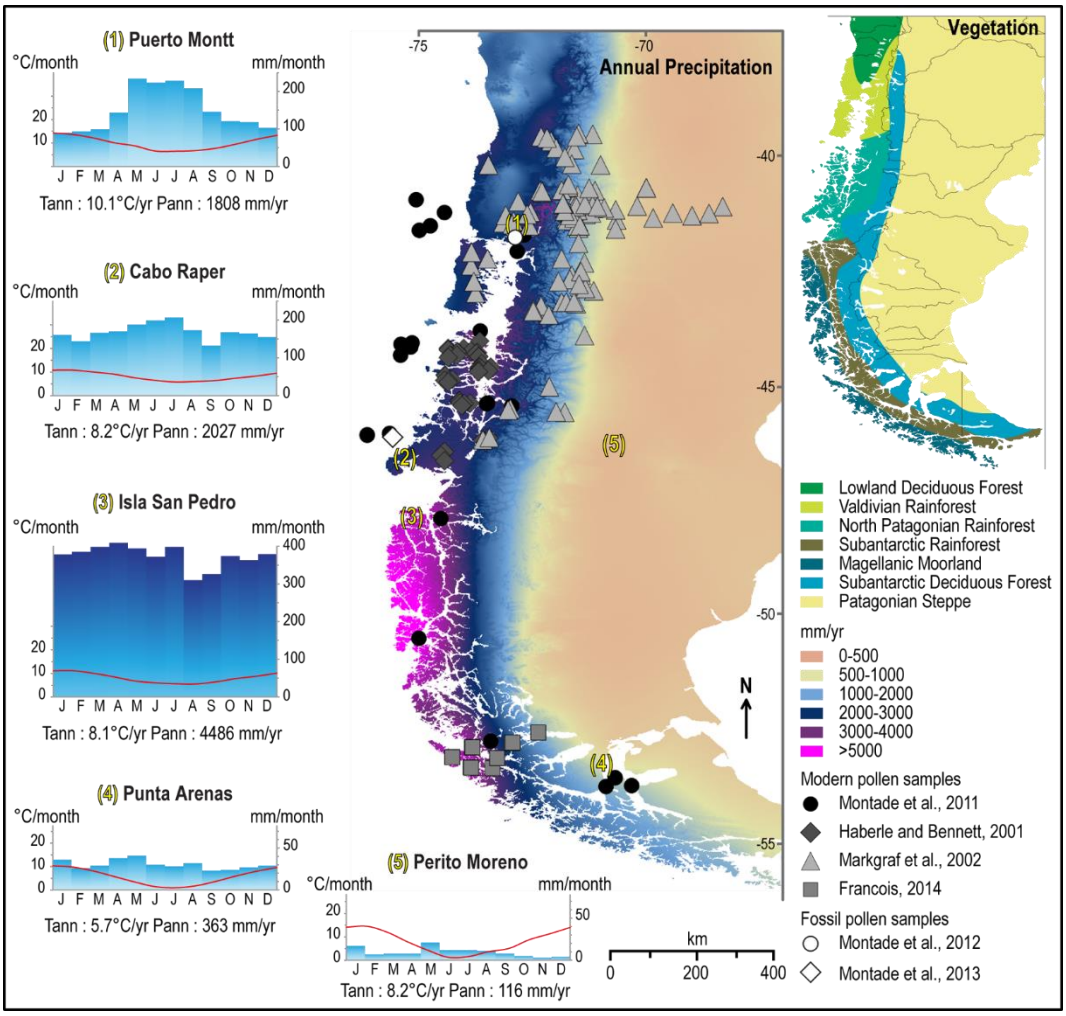

Figure 1. Climate and vegetation maps from Patagonia with location of modern samples and fossil pollen records used in this study. Precipitation data were obtained from WorldClim database (Hijmans *et al.*, 2005), climatographs were performed using data from meteorological stations (New_LocClim_1.10 software; Grieser *et al.*, 2006) and vegetation distribution is adapted from Schimithüsen (1956).

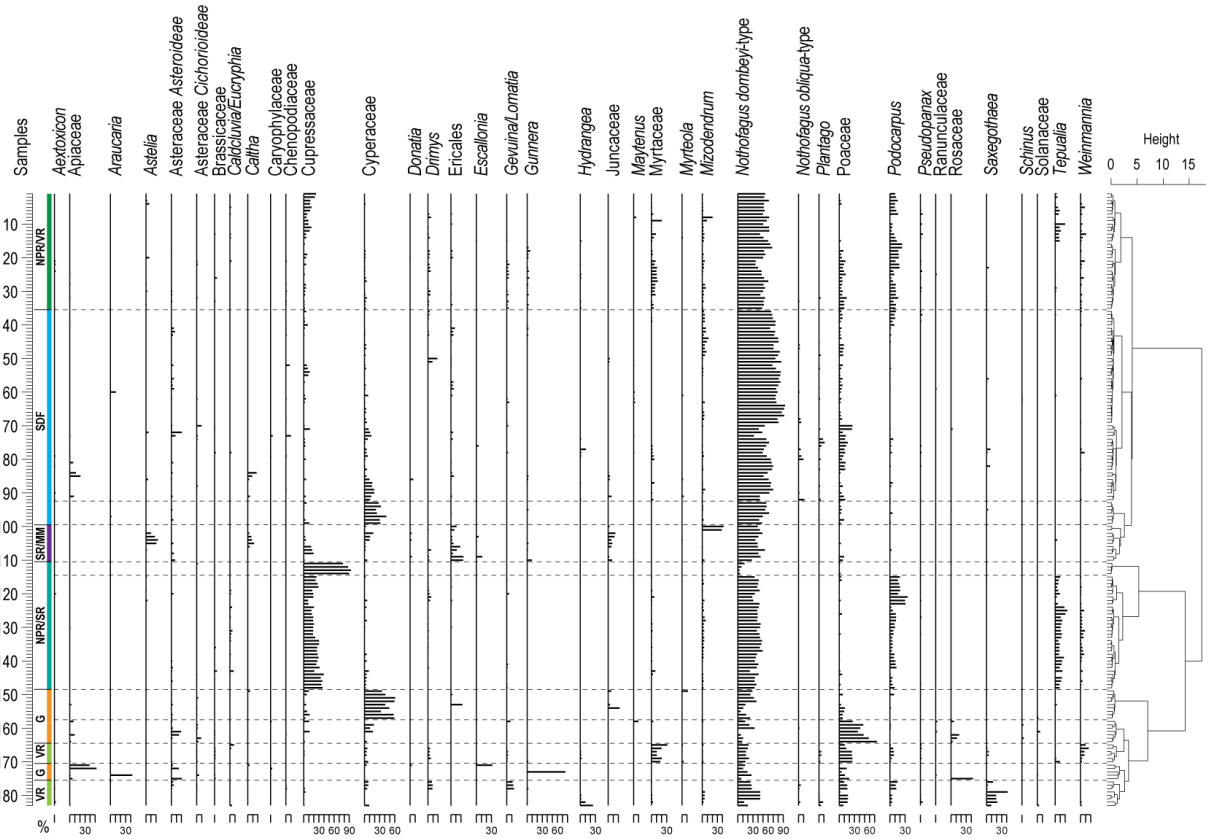

Figure 2. Pollen diagram of the 183 modern pollen samples from western Patagonia showing the main pollen taxa. Ordination of modern pollen samples with pollen zones have been made using a cluster analysis based on chord distance. According to the pollen assemblages of each zone, six vegetation groups were identified: Grassland (G), Subantarctic Deciduous Forest (SDF), Valdivian Rainforest (VR), North Patagonian/Valdivian Rainforest (NPR/VR), North Patagonian/Subantarctic Rainforest (NPR/SR), Subantarctic Rainforest/Magellanic Moorland (SR/MM).

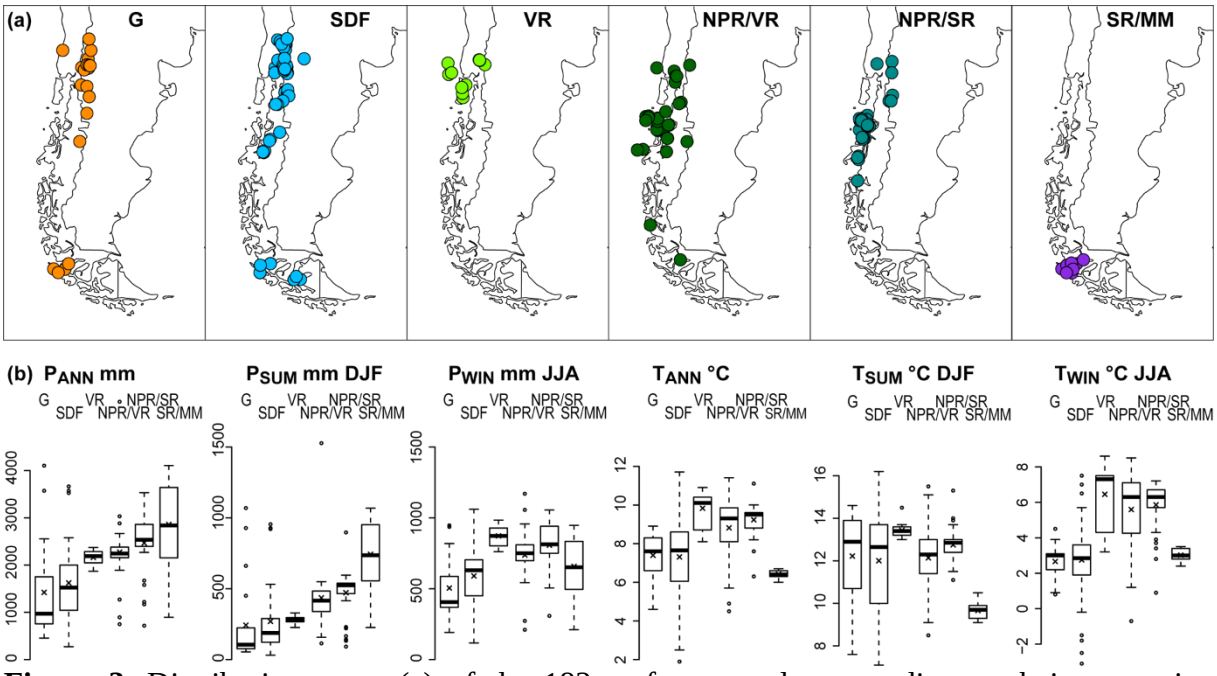

Figure 3. Distribution maps (a) of the 183 surface samples according to their respective vegetation groups attributed from pollen assemblages: Grassland (G), Subantarctic Deciduous Forest (SDF), Valdivian Rainforest (VR), North Patagonian/Valdivian Rainforest (NPR/VR), North Patagonian/Subantarctic Rainforest (NPR/SR), Subantarctic Rainforest/Magellanic Moorland (SR/MM). Boxplots (b) represent the main climate parameters of present-day climate as they relate to the different vegetation groups: P_{ANN} and T_{ANN} correspond respectively to the annual precipitation and the mean annual temperature, P_{SUM} and P_{WIN} correspond respectively to the precipitation sum of December-January-February and June-July-August, T_{SUM} and T_{WIN} correspond to mean temperature of the same months as P_{SUM} and P_{WIN}. The cross on each boxplot indicates the mean value for each climate parameter.

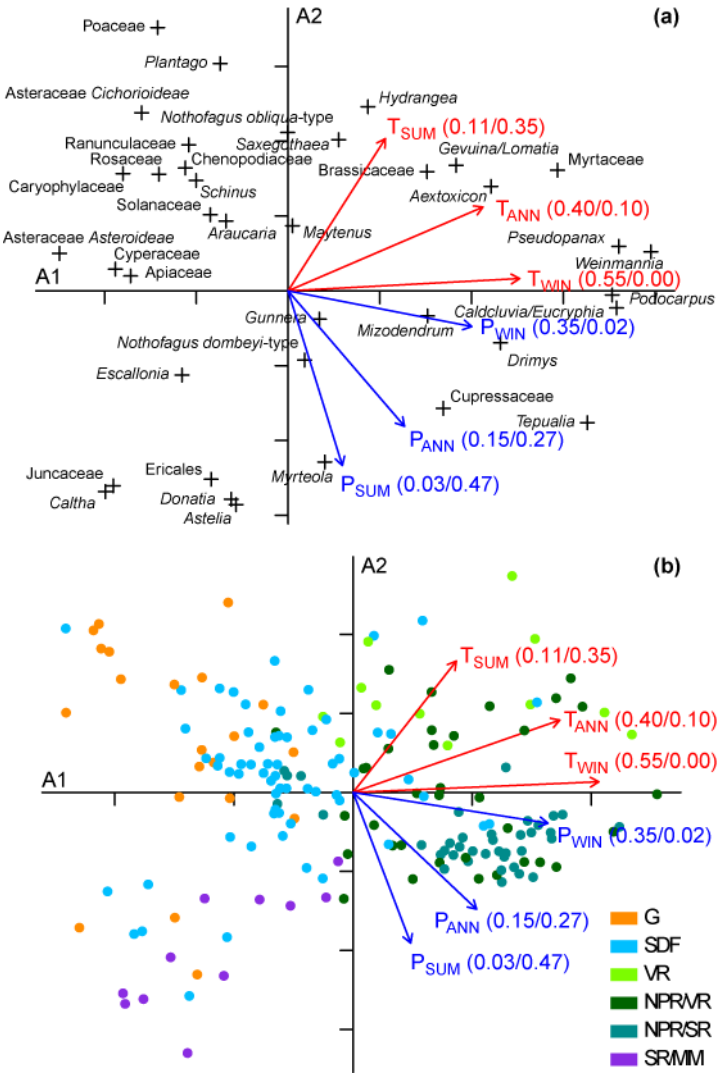

Figure 4. Bi-plot of the principal component analysis (PCA) with the 38 selected pollen taxa (a) and the 183 selected modern pollen samples (b). Eigenvalues for the first and second axes represent respectively 14% and 13% of the total variation. The arrows indicate the passive climate parameter projected in the axes 1-2 bi-plot of the PCA with their respective r^2: P_{ANN} and T_{ANN} correspond respectively to the annual precipitation and the mean annual temperature, P_{SUM} and P_{WIN} correspond respectively to the precipitation sum of December-January-February and June-July-August, T_{SUM} and T_{WIN} correspond to mean temperature of the same months as P_{SUM} and P_{WIN}. Grassland (G), Subantarctic Deciduous Forest (SDF), Valdivian Rainforest (VR), North Patagonian/Valdivian Rainforest (NPR/VR), North

719 Patagonian/Subantarctic Rainforest (NPR/SR), Subantarctic Rainforest/Magellanic Moorland
720 (SR/MM).

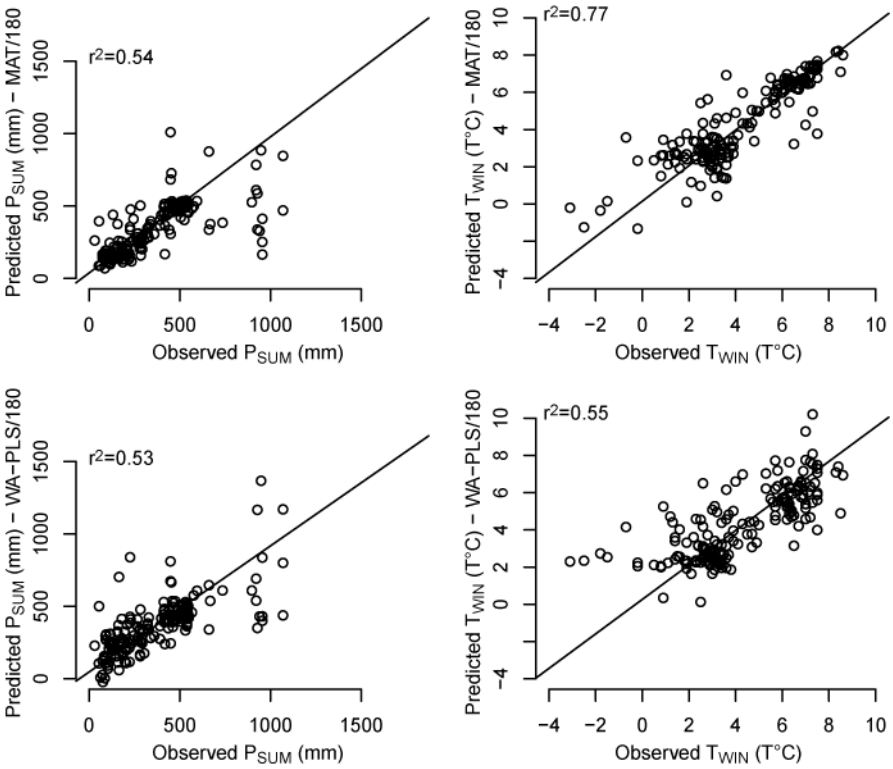

721

722 **Figure 5.** Comparison of predicted versus observed P_{SUM} (precipitation sum of December-
723 January-February) and T_{WIN} (mean temperature from June to August) performed on the 180
724 samples including oceanic and terrestrial pollen data from western Patagonia (excluding three
725 outliers) and using the Modern Analog Technique (MAT) and the Weighted Averaging Partial
726 Least Squares (WA-PLS).

727

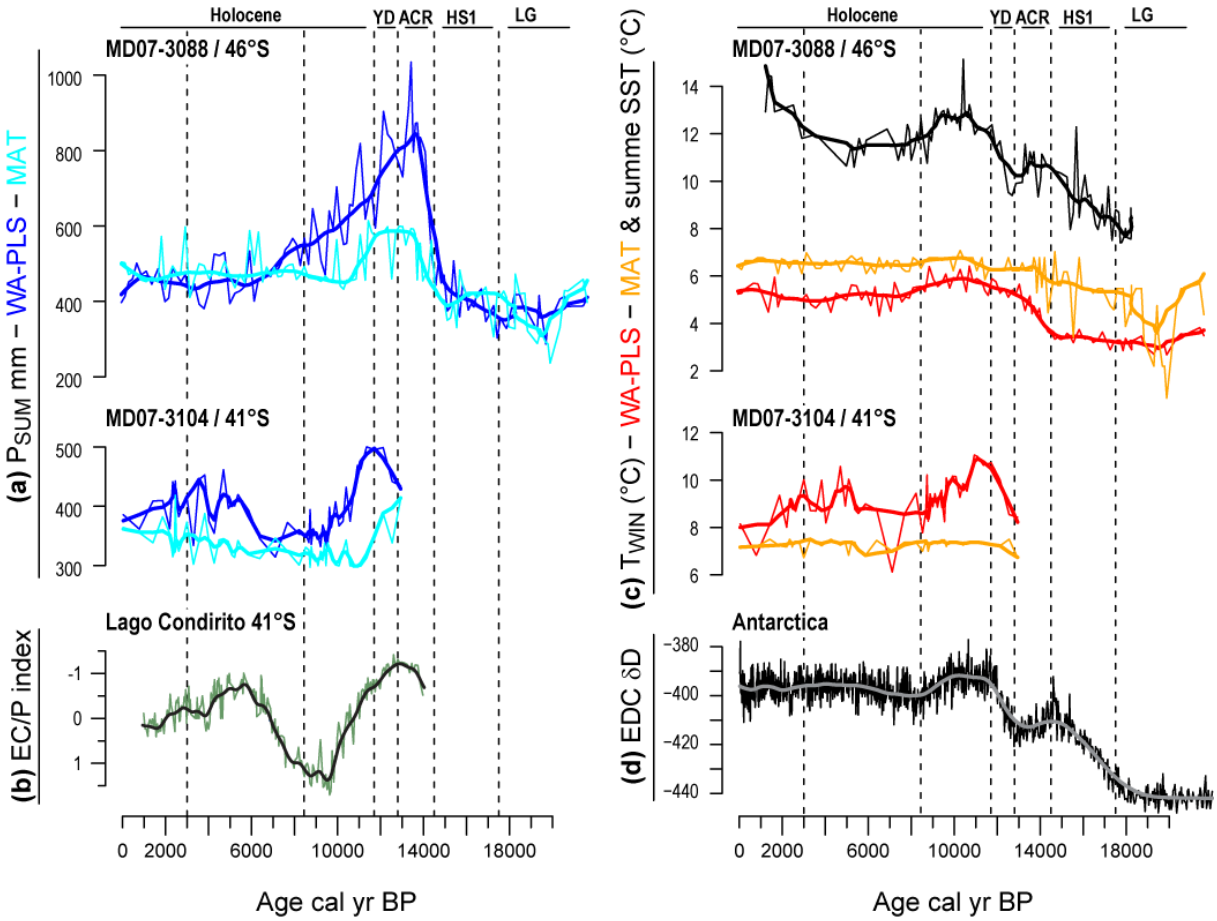

Figure 6. Climate reconstructions from core MD07-3088 and core MD07-3104 compared with independent palaeoclimatic proxies. The P_{SUM} (precipitation sum of December-January-February) and T_{WIN} (mean temperature from June to August) have been reconstructed using the MAT (Modern Analog Technique) and the WA-PLS (Weighted Averaging Partial Least Squares) with the pollen-climate training set of 180 samples. (a) P_{SUM} from core MD07-3088 and MD07-3104; (b) EC/P (*Eucryphia-Caldcluvia*/*Podocarpus*) index from Lago Condorito (Moreno, 2004); (c) SSTs (Summer Sea Surface Temperatures) from core MD07-3088 based on planktonic foraminifera assemblages (Siani *et al.*, 2013) with T_{WIN} from core MD07-3088 and MD07-3104; (d) Ice-core δD based on the age scale of Lemieux-Dudon *et al.* (2010). The original data were fit with a cubic smoothing spline (bold lines). YD, Younger Dryas; ACR, Antarctic Cold Reversal; HS1, Heinrich Stadial 1; LGM, Last Glacial Maximum.

741 **Table 1.** Performance of the Weighted Averaging Partial Least Squares (WA-PLS) and the
742 Modern Analog Technique (MAT) based on leave-one-out cross-validation with 183 and 180
743 samples including oceanic and terrestrial pollen data from western Patagonia (P_{SUM},
744 precipitation sum of December-January-February; T_{WIN}, mean temperature from June to
745 August). The table indicate the best selected component for each parameter and cross-
746 validation test.

747

Model	Component	Variables	Range	r^2	RMSEP	RMSEP % of gradient	Maximum Bias	Average Bias
MAT-183	-	P_{SUM}	31-1527 mm	0.49	180.8	12.1	1035	17.50
WA-PLS-183	2	P_{SUM}	31-1527 mm	0.44	193.3	12.9	925	2.62
MAT-183	-	T_{WIN}	-3.1-8.6 °C	0.77	1.1	20.3	2.1	2.08
WA-PLS-183	2	T_{WIN}	-3.1-8.6 °C	0.56	1.6	28.2	5.1	-0.05
MAT-180	-	P_{SUM}	31-1069 mm	0.54	162	15.6	446	17.31
WA-PLS-180	2	P_{SUM}	31-1069 mm	0.53	164	15.8	266	-0.28
MAT-180	-	T_{WIN}	-3.1-8.6 °C	0.77	1.1	20.4	2.1	-0.04
WA-PLS-180	2	T_{WIN}	-3.1-8.6 °C	0.55	1.6	28.5	5.1	-0.05

748

749

Supporting Information

Figure S1. Comparison between observed and reconstructed present-day climate parameters performed on the 24 modern oceanic pollen samples with the terrestrial pollen dataset including 159 samples. The two climate parameters P_{SUM} (precipitation sum of December-January-February) and T_{WIN} (mean temperature from June to August) are indicated from north to south with their respective r^2 between the observed and reconstructed values. MAT, Modern Analog Technique; WA-PLS, Weighted Averaging Partial Least Squares.

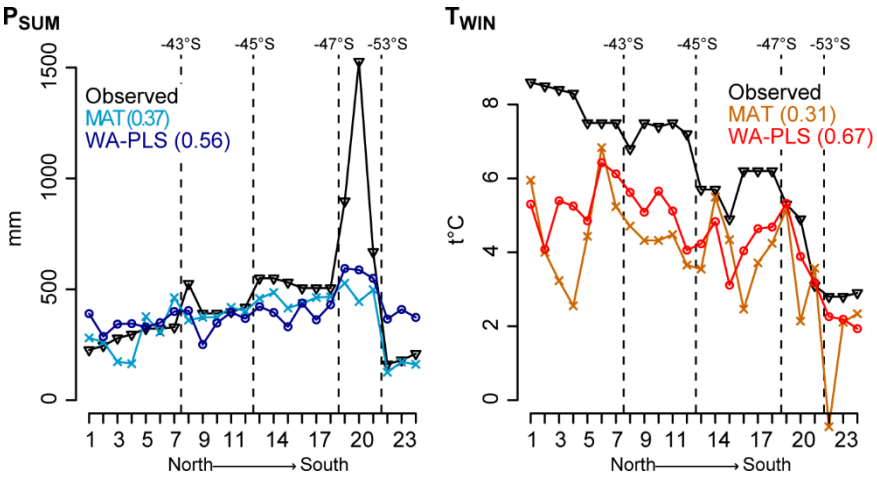

Figure S2. Comparison of predicted versus observed P_{SUM} (precipitation sum of December-January-February) and T_{WIN} (mean temperature from June to August) performed on the 183 samples including oceanic and terrestrial pollen data from western Patagonia and using the Modern Analog Technique (MAT) and the Weighted Averaging Partial Least Squares (WA-PLS). Samples indicated in red correspond to the outliers identified from P_{SUM} and removed of the second 180-training set.

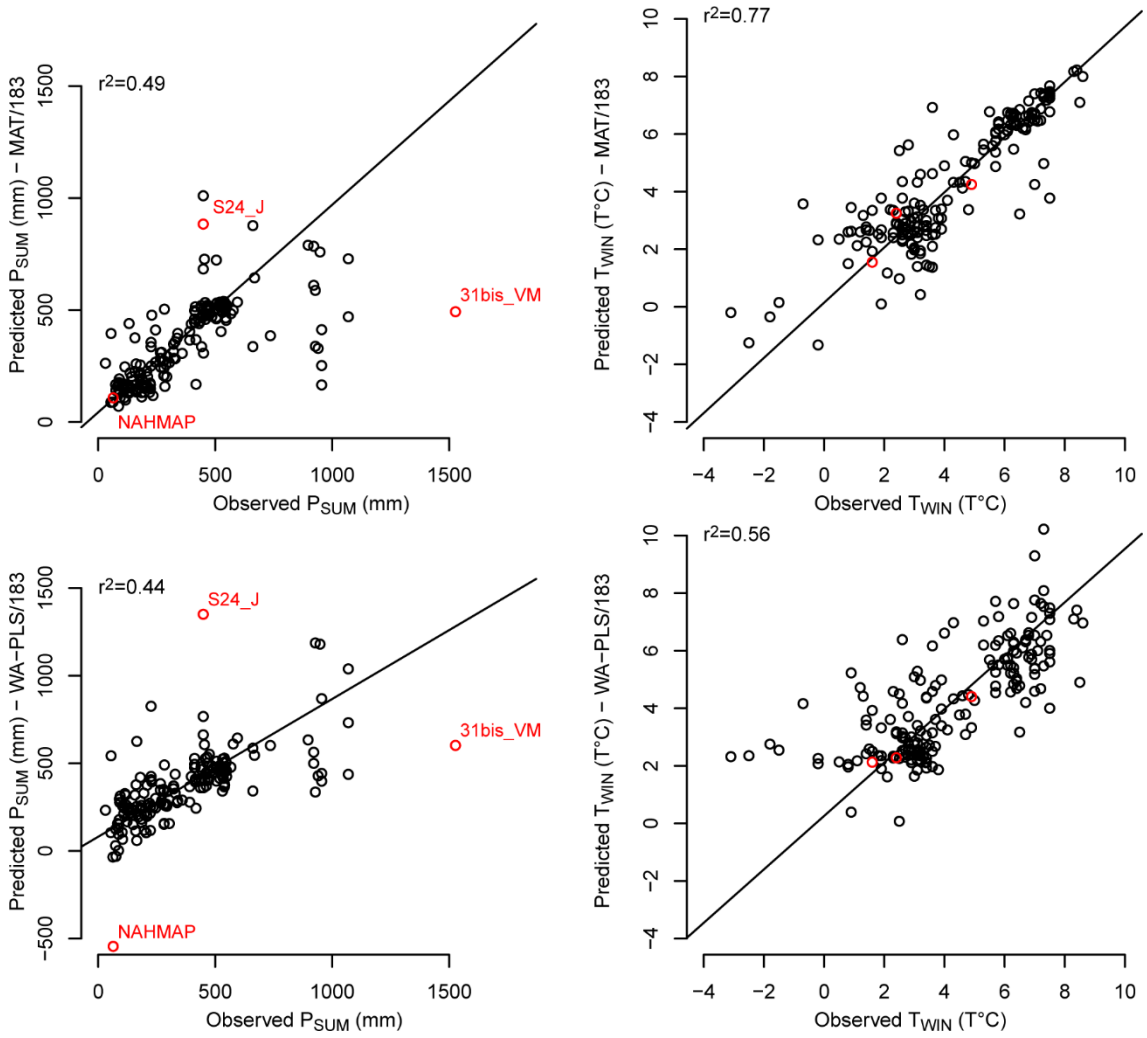

Figure S3. Effect of transfer function r^2 of deleting sites at random (mean of 10 trials; open circles) and from the geographical and environmental neighbourhood of the test site (filled circles and crosses) during cross-validation for the 180-training set. P_{SUM}, precipitation sum of December-January-February; T_{WIN}, mean temperature from June to August; MAT, Modern Analog Technique; WA-PLS, Weighted Averaging Partial Least Squares.

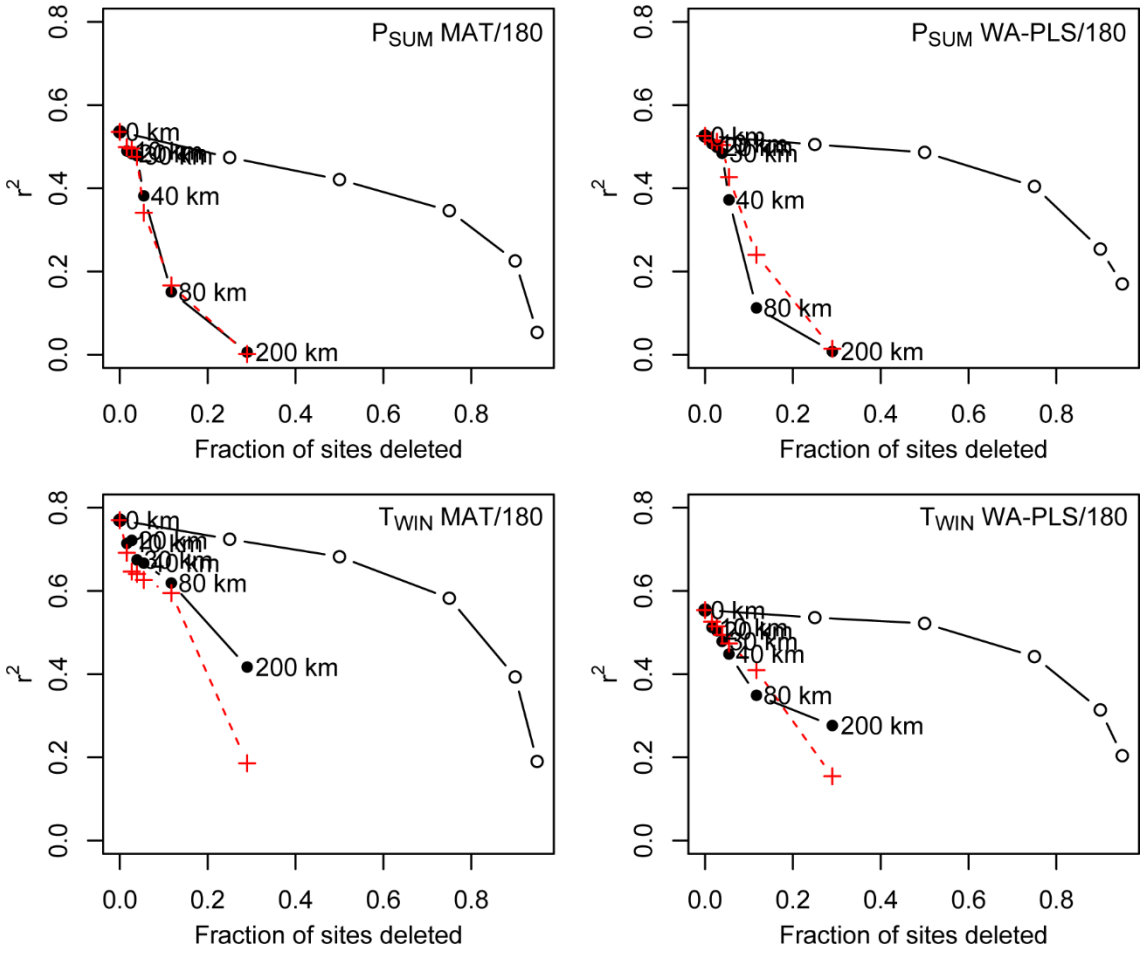

Table S1. List of the surface pollen samples from southern Patagonia according to their location (Long., east longitude and Lat., north latitude) and altitude (m asl). The column 'code' indicate the order of samples in the pollen diagram perform by the cluster analysis (samples without code correspond to samples excluded to perform statistical analyses). The type correspond to oceanic (O), soil (S) and lake (L) samples. Reference (Ref.) to publication 1 (Montade *et al.*, 2011), 2 (Haberle and Bennett, 2001), 3 (Francois, 2014) and 4 (Markgraf *et al.*, 2002). Vegetation groups: Grassland (G), Subantarctic Deciduous Forest (SDF), Valdivian Rainforest (VR), North Patagonian/Valdivian Rainforest (NPR/VR), North Patagonian/Subantarctic Rainforest (NPR/SR), Subantarctic Rainforest/Magellanic Moorland (SR/MM), Indeterminate (Ind).

Name	Code	Type	Long.	Lat.	m asl	Ref.	Vegetation
7_VM	28	O	-76.1	-46.07	0	1	NPR/VR
8_VM	30	O	-76.1	-46.08	0	1	NPR/VR
11_VM	34	O	-75.37	-44.33	0	1	NPR/VR
12_VM	24	O	-75.36	-44.09	0	1	NPR/VR
13bis_VM	31	O	-75.15	-44.15	0	1	NPR/VR
14ter_VM	33	O	-74.41	-41.21	0	1	NPR/VR
15_VM	176	O	-75.03	-40.93	0	1	VR
16_VM	177	O	-74.96	-41.6	0	1	VR
17_VM	178	O	-74.72	-41.5	0	1	VR
18bis_VM	21	O	-72.78	-41.71	0	1	NPR/VR
19ter_VM	35	O	-72.67	-41.7	0	1	NPR/VR
20_VM	22	O	-72.82	-42.06	0	1	NPR/VR
21_VM	25	O	-75.12	-44.06	0	1	NPR/VR
22_VM	23	O	-73.63	-43.8	0	1	NPR/VR
23bis_VM	19	O	-73.47	-45.38	0	1	NPR/VR
24_VM	29	O	-73.49	-45.39	0	1	NPR/VR
26_VM	39	O	-72.94	-45.44	0	1	SDF
27_VM	18	O	-75.61	-46.04	0	1	NPR/VR
30_VM	122	O	-74.49	-47.9	0	1	NPR/SR
31bis_VM	20	O	-74.97	-50.52	0	1	NPR/VR
33_VM	107	O	-73.4	-52.77	0	1	SR/MM
36_VM	42	O	-70.88	-53.76	0	1	SDF
37_VM	43	O	-70.68	-53.57	0	1	SDF
38_VM	41	O	-70.32	-53.74	0	1	SDF
1_SH	132	L	-73.64	-44.02	25	2	NPR/SR
2_SH	10	L	-74.33	-44.18	75	2	NPR/VR
3_SH	131	L	-73.99	-44.18	30	2	NPR/SR

4_SH	13	L	-74.33	-44.21	75	2	NPR/VR
5_SH	136	L	-74.33	-44.21	75	2	NPR/SR
6_SH	11	L	-74.33	-44.21	75	2	NPR/VR
7_SH	127	L	-73.83	-44.24	50	2	NPR/SR
8_SH	145	L	-74.13	-44.25	49	2	NPR/SR
9_SH	128	L	-74.13	-44.26	47	2	NPR/SR
10_SH	138	L	-73.69	-44.27	75	2	NPR/SR
11_SH	133	L	-73.72	-44.29	75	2	NPR/SR
12_SH	125	L	-73.72	-44.29	75	2	NPR/SR
13_SH	124	L	-74.28	-44.33	10	2	NPR/SR
14_SH	129	L	-74.29	-44.33	10	2	NPR/SR
15_SH	146	L	-74.14	-44.33	25	2	NPR/SR
16_SH	134	L	-73.66	-44.36	50	2	NPR/SR
17_SH	137	L	-73.66	-44.36	50	2	NPR/SR
18_SH	135	L	-73.66	-44.36	50	2	NPR/SR
19_SH	12	L	-74.33	-44.38	125	2	NPR/VR
20_SH	139	L	-73.6	-44.52	76	2	NPR/SR
21_SH	14	L	-73.4	-44.59	20	2	NPR/VR
22_SH	115	L	-73.65	-44.59	30	2	NPR/SR
23_SH	147	L	-73.63	-44.6	30	2	NPR/SR
24_SH	140	L	-73.6	-44.63	20	2	NPR/SR
25_SH	126	L	-73.66	-44.66	400	2	NPR/SR
26_SH	130	L	-73.45	-44.67	25	2	NPR/SR
27_SH	3	L	-73.67	-44.69	750	2	NPR/VR
28_SH	4	L	-73.67	-44.69	770	2	NPR/VR
29_SH	1	L	-74.4	-44.76	25	2	NPR/VR
30_SH	5	L	-74.39	-44.78	25	2	NPR/VR
31_SH	6	L	-74.24	-44.86	75	2	NPR/VR
32_SH	119	L	-74.33	-44.88	25	2	NPR/SR
33_SH	7	L	-74.41	-44.88	25	2	NPR/VR
34_SH	2	L	-74.33	-44.92	75	2	NPR/VR
35_SH	148	L	-74.1	-45.33	25	2	NPR/SR
36_SH	116	L	-74.08	-45.33	125	2	NPR/SR
37_SH	117	L	-74.07	-45.37	25	2	NPR/SR
38_SH	120	L	-73.85	-45.38	25	2	NPR/SR
39_SH	141	L	-73.98	-45.39	85	2	NPR/SR
40_SH	142	L	-74.03	-45.43	25	2	NPR/SR
41_SH	36	L	-73.44	-46.14	120	2	SDF
42_SH	16	L	-73.57	-46.18	825	2	NPR/VR
43_SH	40	L	-73.58	-46.19	675	2	SDF
44_SH	37	L	-73.51	-46.23	75	2	SDF
45_SH	118	L	-74.41	-46.44	25	2	NPR/SR
46_SH	123	L	-74.49	-46.52	25	2	NPR/SR
47_SH	121	L	-74.41	-46.64	25	2	NPR/SR
S38_J	153	S	-74.24	-53.12	2	3	G
S39(2)_J	102	S	-74.24	-53.12	78	3	SR/MM

S39(1)_J	103	S	-74.24	-53.12	78	3	SR/MM
S32_J	171	S	-73.84	-53.34	378	3	G
S29_J	109	S	-73.83	-53.35	2	3	SR/MM
S31_J	72	S	-73.84	-53.34	324	3	SDF
S30_J	61	S	-73.83	-53.35	70	3	SDF
S28_J	50	S	-73.83	-53.35	12	3	SDF
S34_J	100	S	-73.36	-53.36	26	3	SR/MM
S16_J	84	S	-73.81	-52.9	290	3	SDF
S9_J	104	S	-73.8	-52.91	30	3	SR/MM
S21_J	91	S	-73.81	-52.9	256	3	SDF
S4_J	101	S	-73.8	-52.9	155	3	SR/MM
S36_J	149	S	-73.26	-53.14	6	3	G
S35_J	108	S	-73.26	-53.14	30	3	SR/MM
S25_J	85	S	-72.94	-52.81	411	3	SDF
S24_J	105	S	-72.93	-52.81	90	3	SR/MM
S26_J	106	S	-72.93	-52.81	13	3	SR/MM
S23_J	86	S	-72.93	-52.81	22	3	SDF
S42_J	173	S	-72.94	-52.81	53	3	G
S27_J	51	S	-72.92	-52.8	12	3	SDF
S41_J	110	S	-72.36	-52.58	4	3	SR/MM
S40_J	8	S	-72.36	-52.58	14	3	NPR/VR
AGUICER	74	S	-72.12	-45.02	270	4	SDF
ALEBOG	15	S	-72.9	-41.4	100	4	NPR/VR
ALEMIT	70	S	-71.42	-42.58	1000	4	SDF
ALENOR	54	S	-71.63	-42.58	800	4	SDF
ANGOST	111	S	-71.5	-40.83	800	4	NPR/SR
ANTILL	82	S	-72.28	-40.75	730	4	SDF
AUSESQ	112	S	-71.45	-42.83	1100	4	NPR/SR
BAYAS		S	-70.65	-41.37	1100	4	G
CANAMOS	62	S	-71.48	-41.55	700	4	SDF
CARILAF	79	S	-71.63	-39.83	875	4	SDF
CASOVE	151	S	-71.8	-41.18	870	4	G
CERDIE15	57	S	-71.65	-41.3	1500	4	SDF
CERDIE17	81	S	-71.65	-41.3	1750	4	SDF
CERDIE18	56	S	-71.65	-41.3	1800	4	SDF
CEZARE	95	S	-71.67	-41.3	1150	4	SDF
CHALL	152	S	-71.32	-41.25	1250	4	G
CHEQUE		S	-70.67	-41.57	1400	4	G
CHILBORD	48	S	-71.75	-40.67	1000	4	SDF
COLOP	64	S	-71.57	-41.1	1500	4	SDF
COMALLO		S	-70.2	-41.07	815	4	G
CONDOR		S	-71.15	-41.12	800	4	SR/MM
CONFLUEN		S	-71.12	-40.73	690	4	SR/MM
DDTRELA	98	S	-71.7	-40.65	850	4	SDF
ELTEPU		S	-73.13	-41.43	100	4	SR/MM
EPUYZ	163	S	-71.35	-42.31	800	4	G

ESPERA	159	S	-71.85	-42.22	550	4	G
ESQAER	172	S	-71.15	-42.92	780	4	G
ESTGRA		S	-70.67	-41.15	980	4	G
FARWES	156	S	-71.2	-41.22	800	4	G
FUTALE1		S	-71.53	-43.2	380	4	G
FUTALE2	75	S	-71.85	-43.17	330	4	SDF
FUTBOR	113	S	-71.75	-43.17	490	4	NPR/SR
GUALALA	77	S	-72.08	-39.65	450	4	SDF
INGJAC1		S	-69	-41.28	870	4	G
INGJAC2		S	-69.85	-41.33	960	4	G
LANQUIH	143	S	-72.8	-40.97	150	4	NPR/SR
LANQUIV	76	S	-72.53	-41.2	66	4	SDF
LAOLAO	44	S	-71.55	-41.05	765	4	SDF
LAUFCH		S	-69.42	-41.22	800	4	G
LAZETA	164	S	-71.35	-43.9	760	4	G
LGNVER	68	S	-71.57	-39.83	400	4	SDF
LGOCAM	45	S	-71.85	-40.72	1000	4	SDF
LGOCAS	32	S	-71.78	-45.58	1000	4	NPR/VR
LGOCC	17	S	-73.57	-46.18	820	4	NPR/VR
LGOCOR1	65	S	-71.7	-40.6	810	4	SDF
LGOCOR2	73	S	-71.33	-42.87	750	4	SDF
LGOESP	182	S	-72.32	-40.73	525	4	VR
LGOFON	66	S	-71.75	-41.35	750	4	SDF
LGOGAL	83	S	-70	-40.67	950	4	SDF
LGOGUI		S	-71.48	-41.42	950	4	SR/MM
LGOHES	88	S	-71.73	-41.38	740	4	SDF
LGOLAR	63	S	-71.67	-42.67	750	4	SDF
LGOMAL	87	S	-72.33	-43.38	1000	4	SDF
LGOMIR	38	S	-73.43	-46.13	115	4	SDF
LGOMOR	144	S	-71.52	-41.5	800	4	NPR/SR
LGOMOS	71	S	-71.43	-42.5	600	4	SDF
LGONELT	92	S	-71.97	-39.8	200	4	SDF
LGOPAS	165	S	-73.83	-42.37	150	4	VR
LGOPAT		S	-70	-40.67	950	4	Ind
LGOPID		S	-73.07	-41.27	170	4	G
lGOPOP	169	S	-73.47	-42.22	115	4	VR
LGORIE		S	-72.97	-45.5	250	4	G
LGOSAR	78	S	-72.56	-41.5	400	4	SDF
LGOSCH	58	S	-71.5	-41.16	2100	4	SDF
LGOTAR1	167	S	-73.77	-42.72	100	4	VR
LGOTAR2	168	S	-73.77	-42.72	100	4	VR
LGOTOR1	180	S	-72.27	-40.77	700	4	VR
LGOTOR2	181	S	-72.27	-40.77	700	4	VR
LGOTRO	59	S	-71.5	-41.16	2000	4	SDF
LGOVEN1	46	S	-71.67	-41.22	825	4	SDF
LGOVEN2	49	S	-73.02	-45.53	650	4	SDF

LGOVEN3	47	S	-71.67	-41.22	825	4	SDF
LGOYEL	26	S	-72.3	-43.25	546	4	NPR/VR
LLAOL	9	S	-71.55	-41.05	850	4	NPR/VR
LOSCLAR	89	S	-71.82	-41.03	1100	4	SDF
LOSMENU		S	-68.33	-41.08	840	4	G
MALBOO	157	S	-71.58	-41.33	800	4	G
MALLIN	183	S	-72.28	-40.75	750	4	VR
MALLINAU	99	S	-71.68	-41.27	900	4	SDF
MALSON	93	S	-71.53	-41.08	800	4	SDF
MAQUIN		S	-68.63	-41.23	870	4	G
MASCAR	52	S	-71.67	-41.27	800	4	SDF
MATAMOL	161	S	-71	-40.17	1100	4	G
MAUSTR	27	S	-72.47	-43.33	600	4	NPR/VR
MELLIZ		S	-70	-40.67	950	4	Ind
MIRABJ	160	S	-73.45	-40.17	750	4	G
MIRADOR	150	S	-73.45	-40.17	850	4	G
MONTHU	80	S	-71.63	-40.15	640	4	SDF
MYELCH	96	S	-72.47	-43.37	1000	4	SDF
NAHHUA	162	S	-71.17	-41.05	810	4	G
NAHMAP	174	S	-71.17	-39.5	1500	4	G
NAHUH	158	S	-71.34	-41.03	830	4	G
NANTY	114	S	-71.58	-43.17	530	4	NPR/SR
NOTESQ	67	S	-71.47	-42.78	1180	4	SDF
PAMTOR	55	S	-71.45	-41.5	1000	4	SDF
PANQHUE	90	S	-71.78	-40	1100	4	SDF
PASTAHU	170	S	-73.83	-42.37	150	4	VR
PEDREG	154	S	-71.97	-45.57	550	4	G
PILCAN		S	-70.92	-41.11	1000	4	G
PRIMAV	155	S	-71.25	-40.68	800	4	G
PRTMON		S	-72.93	-41.47	100	4	G
PSOTROM	97	S	-71.48	-39.48	11.96	4	SDF
PTOBLES	53	S	-71.8	-41.03	760	4	SDF
PTOCAFE		S	-71.92	-42.72	550	4	SR/MM
PTORAM		S	-72.13	-43.45	300	4	G
QUILLEH	60	S	-71.52	-39.55	1104	4	SDF
REPOL		S	-71.48	-41.88	500	4	SR/MM
RINCON	175	S	-71.07	-41.08	580	4	G
RIOALER	94	S	-71.78	-41.18	850	4	SDF
RIOFRI	179	S	-71.82	-41.02	850	4	VR
RIONEG		S	-73.82	-42.08	60	4	SR/MM
RIOTEP		S	-72.6	-41.25	70	4	G
RUCANAN	69	S	-72.3	-39.55	290	4	SDF
SANANTO	166	S	-73.73	-42.97	150	4	VR
TARAHUB		S	-73.77	-42.72	100	4	G
TRALCAP		S	-72.17	-39.58	230	4	G

Table S2. List of the 78 pollen taxa.

Family	Taxa name
Rosaceae	*Acaena*
Fabaceae	*Adesmia*
Aextoxicaceae	*Aextoxicon*
Apiaceae	Apiaceae
Araucariaceae	*Araucaria*
Elaeocarpaceae	*Aristotelia*
Asteraceae	*Artemisia*
Asteliaceae	*Astelia*
Asteraceae	Asteraceae *Asteroideae*
Asteraceae	Asteraceae *Cichorioideae*
Flacourtiaceae	*Azara*
Berberidaceae	*Berberis*
Boraginaceae	Boraginaceae
Brassicaceae	Brassicaceae
Buddlejaceae	*Buddleja*
Scrophulariaceae	*Calceolaria*
Cunoniaceae	*Caldcluvia/Eucryphia*
Ranunculaceae	*Caltha*
Caryophylaceae	Caryophylaceae
Chenopodiaceae	Chenopodiaceae
Cupressaceae	Cupressaceae
Cyperaceae	Cyperaceae
Podocarpaceae	*Dacrydium*
Columelliaceae	*Desfontainia*
Stylidiaceae	*Donatia*
Winteraceae	*Drimys*
Proteaceae	*Embothrium*
Ephedraceae	*Ephedra*
Ericales	Ericales
Escalloniaceae	*Escallonia*
Euphorbiaceae	Euphorbiaceae
Fabaceae	Fabaceae
Gentianaceae	Gentianaceae
Geraniaceae	Geraniaceae
Proteaceae	*Gevuina/Lomatia*
Griseliniaceae	*Griselinia*
Gunneraceae	*Gunnera*
Hydrangeaceae	*Hydrangea*
Hydrophylaceae	Hydrophylaceae
Juncaceae	Juncaceae
Santalaceae	*Lepidoceras*
Philesiaceae	*Luzuriaga*
Celastraceae	*Maytenus*

Misodendraceae	*Misodendrum*
Apiaceae	*Mulinum*
Myrtaceae	Myrtaceae
Myrtaceae	*Myrteola*
Nothofagaceae	*Nothofagus dombeyi*-type
Nothofagaceae	*Nothofagus obliqua*-type
Onagraceae	Onagraceae
Thymelaeaceae	*Ovidia*
Hydrophyllaceae	*Phacelia*
Philesiaceae	*Philesia*
Plantaginaceae	*Plantago*
Poaceae	Poaceae
Podocarpaceae	*Podocarpus*
Polygonaceae	Polygonaceae
Primulaceae	Primulaceae
Araliaceae	*Pseudopanax*
Ranunculaceae	Ranunculaceae
Rhamnaceae	Rhamnaceae
Verbenaceae	*Rhaphithamnus*
Grossulariaceae	*Ribes*
Rosaceae	Rosaceae
Rubiaceae	Rubiaceae
Polygonaceae	*Rumex*
Salicaceae	*Salix*
Sapindaceae	Sapindaceae
Podocarpaceae	*Saxegothaea*
Saxifragaceae	Saxifragaceae
Anacardiaceae	*Schinus*
Scrophulariaceae	Scrophulariaceae
Solanaceae	Solanaceae
Myrtaceae	*Tepualia*
Urticaceae	*Urtica*
Valerianaceae	Valerianaceae
Verbenaceae	Verbenaceae
Cunoniaceae	*Weinmannia*

787

788